

# Experimental report

26/04/2022

**Proposal:** 8-02-944

**Council:** 10/2020

**Title:** Interaction of advanced drug delivery vehicles with model biomembranes

**Research area:** Biology

**This proposal is a new proposal**

**Main proposer:** Jayne LAWRENCE

**Experimental team:** Samuel WINNALL  
Richard CAMPBELL

**Local contacts:** Samantha MICCIULLA  
Armando MAESTRO

**Samples:** CHOLESTEROL  
poly(D,L-lactic-co-glycolic acid)/[-poly(ethylene glycol)] (PLGA/PEG) copolymers  
phospholipids including sphingomyelin

<b>Instrument</b>	<b>Requested days</b>	<b>Allocated days</b>	<b>From</b>	<b>To</b>
FIGARO	3	2	21/05/2021	23/05/2021

## **Abstract:**

There has been a shift in the pharmaceutical industry's focus towards development of drugs that act at specific sub-cellular compartments, thereby creating a demand for advanced delivery vehicles that convey their drug payload to the required site of action. A common feature of intracellular drug delivery is that the delivery vehicle is taken up by the target cells via endocytosis with the vehicle becoming engulfed in the endosome. In order for the drug to exert its action, it must escape from the endosome. Neutron reflectometry will help to unravel the interaction(s) between polymeric nanoparticles of interest here and the endosomal membranes (and in particular the early and late stage endosomal membranes) to enable the design of efficient delivery vehicles that can escape the endosome at an early stage with an intact drug payload.

# Final Experiment Report: Interaction of advanced drug delivery vehicles with model biomembranes (#8-02-944)

## Introduction

Most of the emergent therapies from pharmaceutical companies, including precision cell-based therapies, rely for their activity on being delivered directly into the cytosol or alternatively to specific sub-cellular compartments [1,2] within the cell. A common feature of such intracellular delivery is that the vehicle is initially taken up by cells via one or more endocytic mechanisms into the early endosome (Figure 1). The slightly acidic early endosome (pH of  $\sim 6.3$ ) develops into the late endosome, during which change the pH is gradually lowered (pH  $\sim 5.5$ ) by ATPase proton pumps that actively transport protons into the endosome. Thereafter, the late endosome fuses with the lysosome (pH 4–5) and the intraluminal contents are degraded by lysosomal enzymes. In order for the vehicle, and more importantly for the payload it carries, to reach the cytosol, it must escape from the endosomal/lysosomal pathway before it is degraded inside the lysosome, generally by hydrolytic enzymes. Some of the payload may recycle back to the cell surface via the recycling endosome. For most delivery

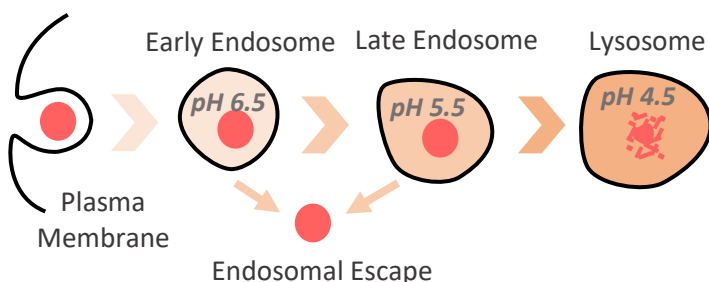


**Fig. 1** Schematic representation of the endocytic uptake and intracellular trafficking of delivery vehicles.

systems, endosomal escape is very inefficient, generally believed to be a few percent or less [3,4]. Consequently, most of the vehicle and its payload are retained inside the endosome/lysosome.

The main goal of experiment #8-02-944 was therefore to elucidate the mechanism(s) by which these vehicles escape from the endosome by neutron reflectometry. Over the past decades, endosomal entrapment has been a major bottleneck in the formulation of intracellularly targeted medicines, where

'smart' nanoparticulate delivery systems have been increasingly studied to ensure the delivery of therapeutic modalities to their intended intracellular site of action. For example, lipid nanoparticles (LNPs) have been increasingly studied to effectively deliver nucleic acids and have recently reached world-wide prominence as the delivery vehicle for the COVID-19 vaccines produced by Moderna and Pfizer/BioNTech [5]. Despite the considerable research effort that has gone into the development of these intelligent delivery systems, the field is currently hindered by a poor understanding of how the vehicles escape the endosome and gain access to the interior (cytosol) of the cell. The aim of experiment #8-02-944 was to study the model early and late endosomal membranes (EEM and LEM respectively), in the absence and presence of LNPs, on FIGARO to unravel the interaction(s) between delivery vehicles and endosomal membranes and facilitate the design of efficient delivery vehicles that can escape from the endosome at an early stage with an intact payload.

## Experiment Details

The beam time of #8-02-944 was performed under severe restrictions imposed by the Covid-19 pandemic and could only be performed as a remote experiment with a limited number of team members on site. This required adjustment of the number of sample changes so that they could be handed by the smaller experimental team. For this reason, we did not study two sizes of LNP as originally planned to explore whether there was any size dependency of the nature of the interaction with the model endosomal membrane. Instead, the time was used to study one size of LNP ( $\sim 100$  nm) and to collect some repeats. However, numerous instrumental problems, such as sample over-illumination and misalignment, cost the majority of the awarded beamtime.

The proposal aimed to obtain structural measurements at a surface pressure of 30 mN/m in 4 contrasts (d-lipid/LNP and h-lipid/LNP each in ACMW and D<sub>2</sub>O) over the full Q-range and kinetic compositional measurements in the 2 ACMW contrasts, at low Q. However, due to the limitations outlined above, only structural data in three contrasts for EEM and two contrasts for LEM were obtained, with two contrasts limited to reduced Q ranges (h-EEM/LNPs in D<sub>2</sub>O: 0.03-0.25 Å<sup>-1</sup>, and d-LEM in ACMW: 0.01-0.05 Å<sup>-1</sup>), Figure 2. The low-Q data were insufficient for a kinetics analysis due to the lack of h/d contrasts in ACMW.

For experiment #8-02-944, the 50 ml Nima trough with four injection holes was set up with a syringe pump. Direct beams and pure solvent calibrations were run for a total of 8 hours but were repeated a further twice (35 min each) due to sample over-illumination and misalignment.

## Data Analysis – Structure

We conducted structural measurements using the full-Q range for each system: EEM and LEM, in four contrasts where three for EEM and two for LEM systems were able to be analysed. Each structural measurement first studied the reference monolayer (10 min angle 1,  $\alpha_1$ ; 40 min  $\alpha_3$ ) before injecting the 1 ml LNP sample (35  $\mu$ l LNPs in 965  $\mu$ l PBS buffer for a trough-polyA concentration of 1  $\mu$ g/ml) via syringe pump at a rate of 0.2 ml/min. The kinetics were then measured for 240 min at  $\alpha_3$  to ensure LNP-monomer equilibration, followed by 10 min at  $\alpha_1$  and 40 min at  $\alpha_3$  to resolve the final structure. This resulted in four sets of structural data, i.e. before and after LNP interaction with EEM and LEM monolayers.

All reference measurements, Figure 2(a, c), fitted to a compact stratified layer model: layer 1 with acyl chains, and layer 2 with solvated head groups. Both systems feature an average head group thickness of 10  $\text{\AA}$ , while the EEM system was observed to have a greater average chain thickness of 15.1  $\text{\AA}$ , compared to 12.7  $\text{\AA}$  for LEM, Table (1).

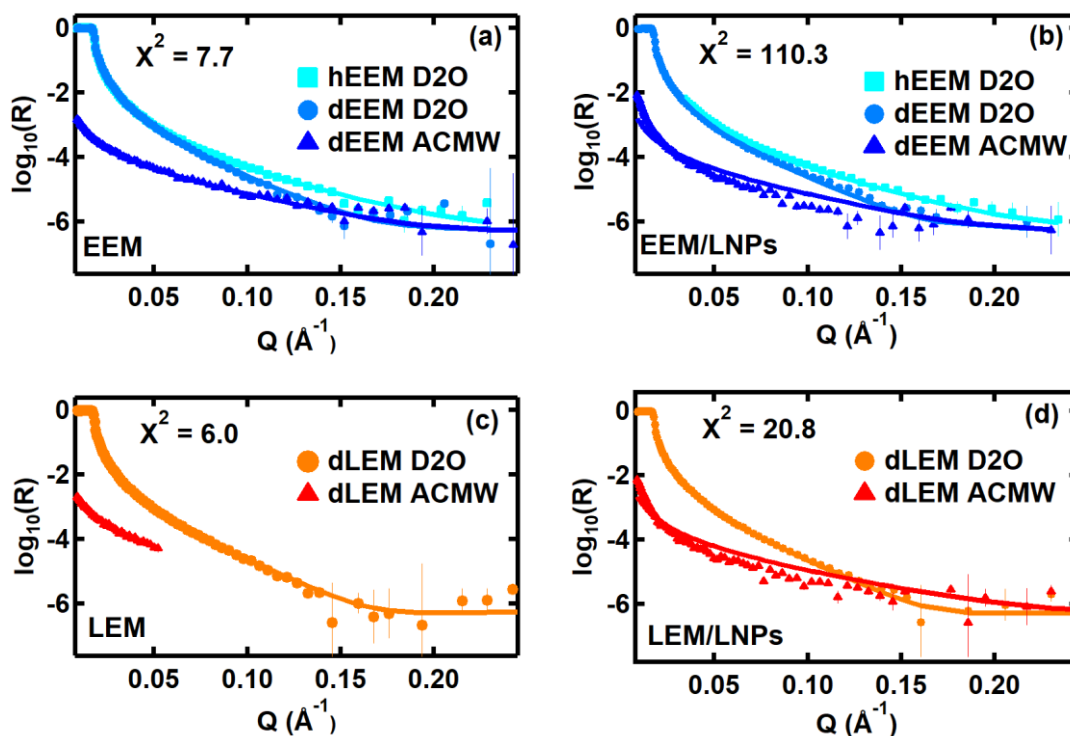


**Fig. 2** Structural neutron reflectivity data for EEM (top) and LEM (bottom) membranes before (left) and after (right) LNP injection in 50 ml of  $D_2O$  and ACMW (8.1% v/v  $D_2O$ ) MES buffers at pH/D 6.5 and pH/D 5.5 (EEM and LEM respectively), at room temperature.  $\chi^2$  increases from 7.7 to 110.3 after LNP injection, and from 6.0 to 20.8, for EEM and LEM respectively, indicating monolayer composition changes upon interaction with LNPs. The injection of 35  $\mu$ l LNPs in 965  $\mu$ l PBS was performed at 0.2 ml/min via syringe pump through four holes at the base of the trough to obtain a trough-polyA concentration of 1  $\mu$ g/ml.

**Table 1** Associated model parameters where chain-layer thickness and backing SLD in  $D_2O$  were fitted, and head-layer thickness was fixed (optimal from thickness range 5-15  $\text{\AA}$ ). The model features an average chain length of 15.1 and 12.7 for EEM and LEM respectively, with both systems having a head group thickness of 10.0  $\text{\AA}$ . Parameters give the reasonable fit in Figure panels 2a and 2c but are insufficient to describe the interaction with LNPs in panels 2b and 2d.

Contrast	Backing SLD	Roughness	Chain Thickness / $\text{\AA}$	Chain SLD	Head Thickness / $\text{\AA}$	Head SLD	%Head Solvent
h-EEM $D_2O$	6.197	3.8	15.1	-0.140	10.0	1.931	63.5
d-EEM $D_2O$	6.213	3.8	15.1	1.401	10.0	1.931	63.5
d-EEM ACMW	0.0	3.8	15.1	1.401	10.0	1.931	63.5
d-LEM $D_2O$	6.186	3.8	12.7	2.076	10.0	1.850	61.8
d-LEM ACMW	0.0	3.8	12.7	2.076	10.0	1.850	61.8

As expected, the reference model parameters presented in Table (1) used to model just EEM and LEM monolayers are insufficient to describe the structure upon equilibration with the LNPs, Figure 2(b, d). This is demonstrated by the 14x and 3x increase in  $\chi^2$  for EEM and LEM respectively and evident in the ACMW contrasts where an upturn in the data at low-Q can be observed, potentially due to trapped aggregates in the film. The insufficiency of the reference model parameters suggests a lipid exchange and/or nucleic acid binding to the head group layer but these contrasts alone are insufficient to accurately determine the interaction. Consequently, we are continuing this research at ISIS by studying the EEM system with deuterated lipids in both the monolayer and the LNP to isolate any lipid exchange. We hope that these data will elucidate the mechanism and allow us to return to #8-02-944 and conclude the analysis.

### Data Analysis – Surface Pressure

In addition to the full-Q structural data, we simultaneously recorded surface pressure. The data, Figure 3, show the spreading of the monolayer solution to a surface pressure  $\sim 30$  mN/m, the first structural measurement, the point of injection and the subsequent kinetics, and final structure. The ACMW contrasts show longer structural measurements due to the reduced count rate and feature a greater upwards drift in surface pressure prior to LNP injection than in the D<sub>2</sub>O contrasts. Additionally, the d-LEM ACMW contrast in Figure 3(b) is observed to spike in pressure after LNP injection as the Wilhelmy plate detaches from the monolayer due to evaporation. Following this, the measurement environment was saturated by placing petri dishes of D<sub>2</sub>O around the Langmuir trough. The remaining contrasts all reached similar surface pressures after LNP equilibration ( $\sim 40$  mN/m), with d-EEM in ACMW demonstrating irregular kinetics does not present in the D<sub>2</sub>O samples. Unfortunately, due to the established limitations, it is not possible to elucidate this behavior from these data alone.

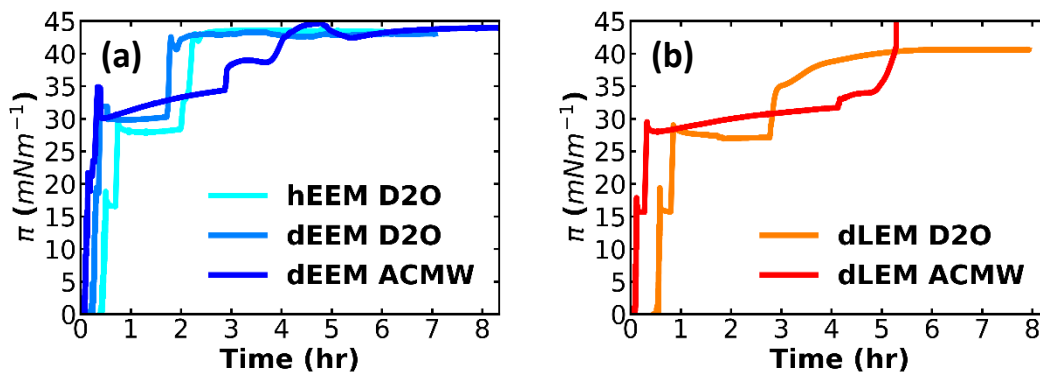


**Fig. 3** Surface pressure,  $\pi$ , injection kinetics for EEM (a) and LEM (b) membranes with LNPs in 50 ml of D<sub>2</sub>O and ACMW (8.1% v/v D<sub>2</sub>O) MES buffers at pH/D 6.5 and 5.5 respectively. The injection of 35  $\mu$ l LNPs in 965  $\mu$ l PBS was performed at 0.2 ml/min via syringe pump through four holes at the base of the trough to obtain a trough-polyA concentration of 1  $\mu$ g/ml. All measurements were performed at room temperature.

### Outlook

Despite numerous technical problems, we were able to record at least 2 contrasts in both EEM and LEM systems, allowing us to estimate the acyl chain and head group thicknesses prior to interaction with LNPs at 30 mN/m. However, further neutron experiments are required to fully elucidate the mechanism(s) of interaction of the LNPs and provide us with enough confidence to publish the collected data. It is anticipated that our work at ISIS, during the ILL long shutdown, will take us closer to understanding the EEM system and the work presented here will support the intended publication and any subsequent application for an LEM continuation study.

### References

1. Stewart et al (2018) Chem. Rev. 118, 7409–7531 |
2. De Geest (2018) Mol. Immunol. 98, 25–27 |
3. Gilleron et al (2013) Nat. Biotechnol. 31, 638–646 |
4. Stewart et al (2016) Nature 538, 183–192 |
5. Buschmann et al (2021) Vaccines 9 65;